Spatial extents of tropical droughts during El Niño in current and future climate in observations, reanalysis, and CMIP5 models

Juan David Perez Arango[1], Benjamin R. Lintner[1], Leila Vespoli Carvalho[2], and Bradfield Lyon[3]

[1]Rutgers, The State University of New Jersey
[2]UC Santa Barbara
[3]University of Maine

November 26, 2022

Abstract

Drought conditions significantly impact human and natural systems in the Tropics. Here, multiple observational and reanalysis products and ensembles of simulations from the Coupled Model Intercomparison Project Phase 5 (CMIP5) are analyzed with respect to drought areal extent over tropical land regions and its past and future relationships to the El Niño/Southern Oscillation (ENSO). CMIP5 models forced with prescribed sea surface temperatures compare well to observations in capturing the present day time evolution of the fraction of tropical land area experiencing drought conditions and the scaling of drought area and ENSO, i.e., increasing tropical drought area with increasing ENSO warm phase (El Niño) strength. The ensemble of RCP8.5 simulations suggests lower end-of-the-century El Niño strength-tropical drought area sensitivity. At least some of this lower sensitivity is attributable to atmosphere-ocean coupling, as historic coupled model simulations also exhibit lower sensitivity compared to the observations.

Spatial extents of tropical droughts during El Niño in current and future climate in observations, reanalysis, and CMIP5 models

Juan D. Perez Arango[1], Benjamin R. Lintner[1,2], Leila M. V. Carvalho[3,4] and Bradfield Lyon[5]

Submitted to *Geophysical Research Letters*

5 April 2021

[1]Department of Environmental Sciences, Rutgers, The State University of New Jersey, New Brunswick, NJ, USA

[2]Rutgers Institute of Earth, Ocean, and Atmospheric Sciences, New Brunswick, NJ, USA

[3]Department of Geography, University of California, Santa Barbara, CA, USA

[4]Earth Research Institute, University of California, Santa Barbara, CA, USA

[5]Climate Change Institute, University of Maine, Orono, ME, USA

---

*Corresponding author: Benjamin R. Lintner, Rutgers, The State University of New Jersey, Department of Environmental Sciences, 14 College Farm Road, New Brunswick, NJ 08901-8551, USA

Email: lintner@envsci.rutgers.edu

Key Points

- Comparison of observed and model-simulated tropical land region drought areal extents show favorable agreement.
- Tropical land region drought area increases with increasing strength of El Niño.
- The apparent decrease in future ENSO-tropical drought area sensitivity appears to arise in part from atmosphere-ocean coupling.

Abstract. Drought conditions significantly impact human and natural systems in the Tropics. Here, multiple observational and reanalysis products and ensembles of simulations from the Coupled Model Intercomparison Project Phase 5 (CMIP5) are analyzed with respect to drought areal extent over tropical land regions and its past and future relationships to the El Niño/Southern Oscillation (ENSO). CMIP5 models forced with prescribed sea surface temperatures compare well to observations in capturing the present day time evolution of the fraction of tropical land area experiencing drought conditions and the scaling of drought area and ENSO, i.e., increasing tropical drought area with increasing ENSO warm phase (El Niño) strength. The ensemble of RCP8.5 simulations suggests lower end-of-the-century El Niño strength-tropical drought area sensitivity. At least some of this lower sensitivity is attributable to atmosphere-ocean coupling, as historic coupled model simulations also exhibit lower sensitivity compared to the observations.

Plain Language Summary

Many regions of the planet are extremely vulnerable to drought. In the tropics, the El Niño/Southern Oscillation (ENSO) phenomenon is recognized as a key driver of drought occurrence. In this study, we analyze the spatial extent of droughts over tropical land regions and evaluate its connection to ENSO in the recent past in observations and current generation models as well as simulated future projections. We demonstrate overall model fidelity in capturing a positive relationship between the tropical land area under drought and El Niño in the recent past and consider how this relationship may change in the future.

Index Terms: Drought (1812), ENSO (4922), Global Climate Models (1626), Tropical Dynamics (3373), Climate Variability (1616)

1) Introduction

Tropical rainfall extremes have significant repercussions for the human and natural systems [*Kumar et al.,* 2013]. Interannually, the El Niño/Southern Oscillation (ENSO) strongly modulates tropical rainfall. Furthermore, anthropogenic forcing of climate, from greenhouse gases or other factors, is likely to impact rainfall across multiple timescales. For example, climate model projections of future monthly-mean tropical rainfall indicate increases in both dry and wet extreme monthly accumulations, leading to broadening of the precipitation distribution [*Lintner et al.,* 2012].

Comprehensive assessment of droughts and their associated impacts requires the quantification of multiple facets of their behavior. While drought intensity, duration, and frequency are integral to assessing their impact on human and natural systems, the spatial characteristics of drought, including their areal extent, are also critical. *Lyon* [2004] and *Lyon & Barnston* [2005], hereafter L04 and LB05, respectively, explored the drought areal extents over tropical land and their relationship to ENSO. Using a standardized precipitation index and categorical definitions of drought, L04 and LB05 demonstrated that during ENSO warm phase (El Niño) conditions, spatially coherent and nearly simultaneous droughts develop over tropical land regions. That is, there is an overall increase in total tropical land area during El Niño events.

Given use of climate models for projecting future hydroclimate impacts, evaluating model fidelity in drought simulation is crucial. *Nasrollahi et al.* [2015] analyzed trends in continental drought areas in an ensemble of Coupled Model Intercomparison Project Phase 5 [CMIP5; *Taylor et al.* 2012] models and reported broad similarity in the geographic areas subject to droughts but with disagreement among trends. More recently, *Ukkola et al.* [2018]

evaluated multiple drought metrics both globally and regionally and demonstrated that, despite the high intermodel agreement, CMIP5 models systematically underestimate drought intensity compared to observations. *Langenbrunner & Neelin* [2013] demonstrated CMIP5 model skill in capturing the observed intensity of teleconnected ENSO rainfall anomalies, albeit with generally poor performance in capturing the detailed spatial structure. While *Ukkola et al.* [2018] analyzed several dimensions of drought in CMIP5, they did not explicitly evaluate model fidelity with respect to spatial extent. On the other hand, *Nasrollahi et al.* [2015] evaluated spatial aspects of drought trends but without particular emphasis on ENSO. *Dai et al.* [1998] found the leading mode of variability in the observationally-derived Palmer Drought Severity Index (PDSI) to be significantly positively correlated with ENSO, with some indications of a strengthening relationship over the latter part of the 20^{th} century. *Coelho & Goddard* [2009] considered some aspects of simulated drought extent and related these to teleconnected precipitation responses to ENSO under both current climate and future projections.

Here, we apply the categorical index-based approach of L04 to quantify spatial drought extent aggregated over all tropical land regions in observations, reanalyses, and CMIP5 models. Our first objective is to validate CMIP5 model performance for the observed ENSO-drought area relationship in current climate, while our second objective is to consider the future ENSO-drought area relationship. In light of the possible changes to ENSO with anthropogenic warming, we seek to determine whether the current ENSO-drought area relationship will hold in the future, i.e., do future projections reflect similar drought area increases with the strength of El Niño as in present climate?

Needless to say, multiple definitions of drought are used by the scientific community, with the choice of drought indices often motivated by the particular type or aspect of drought (meteorological, ecological, agricultural, or hydrological) examined [*Wilhite & Glantz*, 1985]. Since we only consider water supply (rainfall) assessed via a standardized rainfall index (SRI), we expect our results to be most directly applicable to meteorological drought. Other drought indices may very well reflect different behavior than what we report below.

2) Data sets and methods

We employ several publically-available gridded observational and reanalysis datasets, including: CPC Merged Analysis of Precipitation [CMAP; *Xie & Arkin*, 1997]; Tropical Rainfall Measuring Mission [TRMM; *Huffman et al.* 2014]; Global Precipitation Climatology Project [GPCP; *Adler et al.* 2003]; Global Precipitation Climatology Centre [GPCC; *Schneider et al.* 2011]; University of Delaware Precipitation [UDel; *Willmott, & Matsuura*, 2001] University of East Anglia [UEA; *Hulme* 1992; *Hulme et al.* 1998]; ERA-Interim [*Dee et al.* 2011]; and Climate Forecast System Reanalysis [CFSR; *Saha et al.* 2010; *Saha et al.* 2012]. The GPCC, UEA, and UDel data sets are based on station observations; CMAP, GPCP, and TRMM are based on merged land observations and satellite data; and CFSR and ERA-Interim are reanalyses.

We also use three model ensembles from CMIP5: N = 29 prescribed SST simulations between January 1979 and December 2005, also known as Atmospheric Model Intercomparison Project (AMIP) simulations [*Taylor et al.* 2012]; N = 22 fully coupled simulations covering January1979-December 2005; and N = 22 fully coupled simulations under the RCP8.5 projection scenario between January 2005 and December 2100. (A summary of model names and acronyms is provided in the supplemental information.) By applying observed SST boundary conditions, the AMIP simulations generally exhibit smaller biases and model spread relative to historic coupled atmosphere-ocean model simulations. The AMIP simulations further allow direct comparison to observed ENSO events, unlike coupled simulations that do not reproduce the observed time evolution of SSTs. AMIP model selection was based on the availability of monthly fields over the observational analysis period; for the other two ensembles, model selection was guided by an interest in analyzing models appearing in both ensembles. For all models, only a single integration is analyzed, even though multiple realizations exist for some models.

In the interest of standardizing our analyses, all observational products and models were regridded to a common 2.5°x2.5° grid via bilinear interpolation. The interpolation procedure likely results in the muting of more extreme behavior, especially given the occasionally sharp spatial gradients present in tropical rainfall. Qualitatively, however, the behavior of the diagnostics described below computed on the regridded versus native resolution is similar.

As in L04, we compute timeseries of monthly SRI at every tropical land pixel. The SRI analyzed, denoted as S_{12}, represents a 12-month sum of weighted, standardized monthly precipitation anomalies in the log of rainfall:

$$S_{12}(i) = \sum_{j=i-12}^{i} \left(\frac{log P_j - \overline{log}\,\overline{P}_j}{\sigma_j}\right) . \frac{\overline{P}_j}{\overline{P_A}} \qquad (1)$$

In (1), i represents each month during January 1980-December 2008 (348 months total), P_j and P_A, represent the monthly precipitation of the j^{th} month in the sum and total annual accumulation, respectively, and overbars represent climatological mean values. σ_j is the monthly standard deviation of $log\,(P)$. Use of $log\,(P)$ yields a distribution closer to Gaussian than P, the distribution of which is often positively skewed [*Lyon & Barnston*, 2005]. The weighting factor, $\frac{\bar{P}_j}{\overline{P_A}}$, representing the climatological monthly fraction of annual precipitation, damps the influence of large standardized anomalies during months with climatologically low rainfall. For the historical simulations and RCP8.5 projections, the climatology used for $\bar{P}_j$ and $\overline{P_A}$, as well as the monthly standard deviations σ_j correspond to January 1979-December 2005 and January 2074-December 2099, respectively.

S_{12} values are further normalized by standard deviation to obtain a dimensionless index of aggregated precipitation deficits (or surpluses), with values typically ranging from −2 to +2. L04 applied equation (1) to gridded monthly-mean precipitation to calculate timeseries of tropical land area fraction subject to selected threshold levels of drought. In what follows, we adopt the same categorical definitions used in L04, namely moderate, intermediate, and severe, defined respectively for index values < -1, <-1.5, and < -2. By construction, the moderate category includes the intermediate and severe categories, and the intermediate category includes the severe category.

We assess model performance by comparing timeseries for categorical drought land area (as percentages of total tropical land area over 30°S-30°N) obtained from individual models and the multimodel ensemble mean (MEM) with the observationally-based (or reanalysis) datasets. The principal metrics considered for model evaluation are temporal correlation, root-mean-square error (RMSE), and linear unidimensional scaling (LUS, [*Hubert et al.,* 2002]). The latter represents an approach for arranging input objects along a single axis; it does so via a linear least-squares minimization procedure applied to a matrix of distances between every pair of objects (the "proximity matrix").

We further quantify the sensitivity of the observed and simulated categorical drought area timeseries to the strength of El Niño via linear regression analysis. As a simple diagnostic of observed (and AMIP) ENSO strength, we consider SST anomalies over the NINO3.4 region (170ºW-120ºW, 5ºS-5ºN): specifically, we use the NOAA's Climate Prediction Center's Oceanic Nino Index (ONI). For the historical and RCP8.5 model ensembles, ONI indices are constructed from each model's unique SST field. Given the use of multiple indices to define ENSO, it is possible that the results and conclusions below would differ based on the index selected.

Finally, we consider histograms of drought area percentage binned according to ONI values, which gives a sense of how drought area scaling varies with the strength of ENSO. Summing the product of the histogram slope with the frequency of occurrence of binned ONI values provides an additional measure of sensitivity.

3) Results and discussion

The top row of Figure 1 depicts timeseries of the three categorical drought areal fractions for all land gridpoints between 30°S-30°N for the analyzed observations and reanalysis products. The most notable characteristic of the time evolution is the pronounced increases in tropical land region drought area fraction across the three drought categories during El Niño conditions (vertical lines), consistent with the findings of L04. Because of the 12-month sum in the definition of S_{12}, the peak drought fractions lag the peak in El Niño by ~6 months. During some El Niño events, between 20-30% of global tropical land area falls under the moderate category, 15-20% under intermediate, and 5-10% under severe. To put the El Niño drought increases into perspective, the time-mean percentages for the three categories are ~15%, ~7.5%, and ~2%; hence, El Niño conditions are frequently associated with expanding the aggregated tropical drought area by a factor of 2 or more relative to climatological expectation.

Mechanistically, L04 explained the increase in drought area with El Niño in terms of the increased stability of the tropical troposphere to precipitating deep convection with the warming, building on the theoretical framework of *Chiang & Sobel* [2002]. In particular, tropospheric warming associated with anomalous diabatic (convective) heating over the ENSO source region in the Pacific spreads rapidly via planetary wave dynamics throughout the entire tropical belt. That precipitation over land decreases in response to El Niño forcing [*Lintner & Chiang* 2007] is qualitatively consistent with the expansion of tropical land fraction experiencing drought. Of course, how reduced rainfall quantitatively translates to greater drought area is not obvious and should be investigated further.

It is clear, however, that not all El Niño events are associated with large increases in drought area. Focusing on, e.g., CMAP (orange lines in Figure 1), the most pronounced increases in drought fraction coincide with the 1982/83, 1991/92, and 1997/98 El Niño events; while not shown here, the 2015/16 El Niño exhibits a similar increase. As L04 and LB05 noted, this likely reflects event-to-event intensity differences—1982/83 and 1997/98 ranked as the strongest 20th century events in terms of peak (December-January-February-mean) SST anomalies, while 2015/16 has been the strongest El Niño to date in the 21st century. However, it may also reflect more subtle differences inherent in the underlying spatial details, or flavor, of ENSO events. In particular, the 1982/83, 1991/92, and 1997/98 events are recognized as so-called Eastern Pacific events, which are characterized by maximum SST anomalies located further to the east than those for Central Pacific events

[*Capotondi et al.* 2015]. The degree to which different ENSO flavors may systematically impact the tropical ENSO teleconnection represents an area of ongoing research interest.

The other observations depicted in Figure 1 reflect time evolution broadly similar to CMAP, although there are clearly differences among the observations across the three categories and across El Niño events. In GPCC (dark blue line), for example, moderate drought extent is of greater magnitude for 1982/83 and 1991/92 but of lesser magnitude for 1997/98 compared to CMAP. Both the UEA (gray) and UofD (red) datasets yield lower amplitude peaks compared to CMAP (or GPCC and GPCP). The two reanalysis products, CFSR and ERA-Interim (dark green and light green, respectively), agree poorly with the observations. Some of the differences among the observations and reanalyses can be tied to specific regional signatures, e.g., GPCC manifests much larger El Niño phase drought area increases over tropical Africa relative to CMAP (not shown). While cursory, our comparison of observations (and reanalyses) illustrates the need for caution in establishing observational benchmarks (or "truth") for model evaluation.

In the AMIP models (Figure 1, bottom row), the MEM timeseries across all three categories (black curves) largely mirror the observed time evolution. To enable more quantitative comparisons of AMIP models to the observations, in Figure 2 we present Taylor plots [*Taylor*, 2001] computed relative to the mean of the five observational products. With the exception of a few models, most of the AMIP models across all three categories are correlated with the observed timeseries at or above the 95th percent confidence interval according to a two-tailed student t-test, and many are correlated at or above the 99th percentile. The observational products themselves are highly mutually correlated, generally at levels exceeding the model correlations shown in Figure 2.

On the other hand, the two reanalysis products are poorly correlated with the observed timeseries (not shown on Figure 2), with many of the AMIP models exceeding the reanalysis correlations. Since these reanalysis products do not assimilate rainfall, comparable performance to the models is not unexpected; for other drought measures that incorporate additional information such as temperature, which reanalysis products do assimilate, better performance relative to the models is likely. Perhaps not surprisingly, the AMIP MEM outperforms nearly all of models individually in terms of correlation and RMSE, i.e., the model errors are likely not systematic, so they cancel in the ensemble averaging.

Figure 2 also presents the results of LUS application to the 30 x 30 proximity matrix of all model to model and model to mean observation pairs for moderate drought conditions. The results displayed here correspond to the arrangement of models and observational mean according to the LUS unidimensional scaling coordinate. Comparing the distribution of models in the Taylor plot for moderate drought to the LUS shows that many of the highest RMSE models, which are also more strongly correlated with the mean observations, occur on the righthand side of the scaling axis. (Note that while the relative positioning in LUS is meaningful, the overall ordering may be reversed.) Although a full exploration of the implications of LUS ordering of the models and observations is beyond the scope of this study, we highlight some aspects in support of its utility as a tool for model intercomparison. For example, models from the same family are typically situated close to one another along the LUS axis, although not necessarily as immediate neighbors. Models 7 and 13 present an interesting contrast, as they appear in the Taylor plot with comparable RMSE and correlation to the observational mean but are well separated along the LUS scaling axis, that is, these models may be viewed as having comparable fidelity to the observational mean even though they may be considered relatively dissimilar according to LUS.

Given the prominent phase relationship evident between ENSO and tropical land region drought area, we next quantify the scaling of drought area to ENSO strength via simple linear regression of the categorical drought extent timeseries against ONI, focusing here on the moderate drought category for simplicity. For the sensitivity values discussed here, uniform sample sizes are considered by selecting different 20-year periods for the observations and each model ensemble, although qualitatively similar results are obtained with nonuniform sample sizes.

For the five observational products, the mean ENSO sensitivity is 3.6±0.5% $^{o}C^{-1}$; inclusion of the CFSR and ERA reanalyses slightly lowers the estimated sensitivity (3.3±0.5% $^{o}C^{-1}$). The mean sensitivity of the AMIP models compares well to the observations (3.3% $^{o}C^{-1}$), albeit with a larger standard deviation (1.7% $^{o}C^{-1}$). In fact, roughly 1/3 of the AMIP models exceed the highest observed sensitivity (GPCC, 4.1% $^{o}C^{-1}$), while another 1/3 fall below the lowest observed sensitivity (UofD, 2.8% $^{o}C^{-1}$). We will further investigate the drought area-El Niño strength relationship below, but for now, we briefly address future RCP8.5 projection of the categorical droughts over tropical land.

Figure 3 depicts timeseries of the three drought categories from the RCP8.5 ensemble over the course of the 21st century. From these timeseries, it is clear that there is little overall consensus on the projected 21st century trends in tropical land region drought fraction. The inconsistent trends in changing tropical land drought area in the RCP8.5 ensemble may be indicative of model-to-model spread in capturing the physical pathways mediating global warming-related precipitation change. While observed global warming is moistening the atmosphere (Chung et al. 2014), and will likely continue to do so, it is not necessarily clear that this should increase rainfall on regional scales. Moreover, the aggregation of S_{12} across different mean climate regimes and wet and dry seasons may contribute to the trend inconsistency, since distinct precipitation change mechanisms may act over different regions or seasons. For example, the so-called wet-wetter/dry-drier paradigm suggests that wet regions (or seasons) will become wetter and dry regions (or seasons) will become drier with warming [*Liu & Allen*, 2013], potentially leading to changes of either sign in tropical drought fraction.

What about the future drought-ENSO relationship in the RCP8.5 models? The estimated sensitivity of (moderate) drought area to ENSO over the last two decades of the 21st century, 1.0±2.1% $^{o}C^{-1}$, is significantly smaller than is observed or simulated by the AMIP models for the recent past. By itself, this lower sensitivity suggests that future El Niño events of a given magnitude may produce *smaller* increases in tropical land drought area than in current climate. However, it is necessary to provide some further context about this apparent lower sensitivity.

First, while the uncertainty in the RCP8.5 mean sensitivity is slightly higher than in the AMIP models (which, as indicated above, is larger than in the observations), approximately one quarter of the RCP8.5 models exhibit *negative* drought area-ENSO sensitivities, in contrast to the AMIP models for which all sensitivities are positive. Although the latitude band over which we compute drought fraction encompasses some regions (e.g., southeastern South America) for which observed El Niño conditions are associated with increasing, rather than decreasing, rainfall—and as such, may contribute to decreasing El Niño phase drought fraction—these areas are unlikely to dominate the aggregated response. Moreover, in the

RCP8.5 simulations, the ONI itself warms in response to anthropogenic forcing: between the 2010s and 2090s, the mean ONI region SST in the RCP8.5 ensemble increases by 2.8±0.9ºC. Thus, the MEM RCP8.5 model projection exhibits ONI SSTs by the end of the 21st century corresponding to a *strong* present day El Niño. Of course, the ONI region warming needs to be considered in terms of widespread warming of the rest of the planet, and thus the shifting threshold for defining El Niño.

We also point out that the mean sensitivity from the historic coupled model ensemble is 1.8±2.1% ºC^{-1}, i.e., higher than the RCP 8.5 projections, but still smaller than the observed (or AMIP) sensitivities. In other words, even under historic forcing conditions, coupled models manifest smaller drought area sensitivities to El Niño strength than the prescribed SST-forcing AMIP models. Thus, the smaller future ENSO sensitivity appears to be explained, at least in part, by the behavior of coupled atmosphere-ocean models. Coupled models are well-known to exhibit biases and errors in tropical Pacific mean state climate (e.g., an excessive cold tongue) that impact the fidelity of ENSO simulation (Guilyardi et al. 2009), although it is not immediately clear what aspects of incorrect simulation of ENSO account for the differences between the historic and AMIP ensembles.

As a final diagnostic, Figure 4a depicts histograms of moderate tropical land drought fraction bin-averaged according to ONI index after subtraction of 10 year (120 month) running means. Removal of the running mean provides a way to account for the shifting baseline of ENSO events in the presence of a warming background. Figure 4b illustrates the normalized occurrence frequencies of binned ONI values for the observations and model ensembles. In general, for ONI>0, the histograms in Figure 4a indicate increasing land drought with increasing ONI, consistent with expectations. Considered over the whole range of ONI, the histograms exhibit some nonlinearity; for ONI>0, there is a hint of nonlinear scaling, with more rapid increase of drought area with progressively warmer ONI region SSTs.

Despite the qualitative agreement of scaling behavior among the observed, AMIP, historic, and RCP8.5 projection histograms, scatter at given values of ONI is evident; in particular, for the RCP8.5 and, to a lesser extent, historic histograms, the bin averages for ONI>1 are systematically lower than for either the observations or AMIP. In fact, the ordering is consistent with the sensitivity estimates derived from the linear regressions. Some small differences are also evident in the ONI occurrence frequencies shown in Figure 4b: the observed (or AMIP) ONI distributions are slightly more negatively skewed than for either the historic or RCP8.5 ensembles, and the small bump in the distribution at moderate to strong El Niño intensities appearing in the observations is not present in the historic or RCP8.5 distributions.

Since the histogram slopes can be viewed as sensitivities over intervals of (detrended) ONI values, we can more directly compare the regression-based sensitivities to sensitivities derived by summing over the product of the histogram slope in each bin (m_i) with the occurrence frequency of ONI per bin (f_i), i.e.,

$$\Lambda = \sum_{i=1}^{N} f_i m_i \tag{2}$$

Applying this to the data shown in Figure 4, we obtain histogram-based sensitivities of 2.4, 2.3, 1.8, and 1.2% $^{\circ}C^{-1}$ for the observations, AMIP, coupled historic, and coupled RCP8.5 ensembles, respectively. That the Λ are lower than the regression-based estimates for the observations and AMIP reflects the fact that this approach emphasizes more frequent values closer to the center of the distribution, which have smaller slope. That said, the coupled historic and RCP8.5 ensembles again exhibit smaller sensitivities than the observations.

4) Summary and conclusions

Motivated by the prior work linking observed tropical drought land fraction to ENSO strength, we apply a categorical drought index approach to analyze ensembles of global climate models from the Coupled Model Intercomparison Project Phase 5 (CMIP5). Our analysis of prescribed sea surface temperature CMIP models (the AMIP ensemble) demonstrates global climate model fidelity in capturing the observed time evolution of bulk tropical drought area and its scaling relationship with ENSO. In particular, both the observations and AMIP models manifest comparable increases in the aggregated percentage of tropical land region experiencing drought conditions during El Niño events.

By considering the RCP8.5 ensemble, we document an apparent decrease in future tropical land drought area sensitivity to ENSO. As we have shown, roughly half of this decrease may be attributed to differences introduced by the coupled model framework, since the ensemble of historic coupled CMIP5 models shows lower sensitivity in comparison to observations (or AMIP models). After accounting for the influence of simulated coupling with an interactive ocean, the residual smaller end of the 21st century drought area sensitivity to ENSO in RCP8.5 may indicate less pronounced impact of the ENSO teleconnection over tropical land regions. Indeed, the effects of widespread anthropogenic warming could potentially counteract some of the El Niño-related drying (through, e.g., moistening of the atmosphere).

On the other hand, the aggregate view of tropical land drought area and its scaling, while facilitating model comparison, obviously neglects the regional nature of droughts. A more variable future hydroclimate will likely enhance drought severity when and where droughts occur; hence, even if a smaller fraction of tropical land experiences drought in response to ENSO forcing, the local impacts may be exacerbated. Furthermore, we have only considered drought area behavior through rainfall "supply": water demand over tropical continents will almost certainly be compounded with future El Niño warming occurring in a warming world.

Acknowledgments

JPA and BRL acknowledge support of National Science Foundation grant AGS-1505198 and BL acknowledges support of National Science Foundation grant AGS-1650037.

Data Availability Statement

The observational, reanalysis, and simulated rainfall data analyzed in this study may be obtained through the following links:

CMAP
National Center for Atmospheric Research
https://rda.ucar.edu/datasets/ds728.1/

TRMM
Goddard Earth Data Sciences and Information Center
https://disc.gsfc.nasa.gov/datasets/TRMM_3B43_7/summary

GPCP
National Centers for Environmental Information
https://www.ncei.noaa.gov/access/metadata/landing-page/bin/iso?id=gov.noaa.ncdc:C00979

UDel
National Oceanic and Atmospheric Administration Physical Sciences Laboratory
https://psl.noaa.gov/data/gridded/data.UDel_AirT_Precip.html

UEA
University of East Anglia Climate Research Unit
https://sites.uea.ac.uk/cru/data

ERA-Interim

European Centre for Medium-Range Weather Forecasts
https://www.ecmwf.int/en/forecasts/datasets/reanalysis-datasets/era-interim

CFSR
National Center for Atmospheric Research
https://rda.ucar.edu/datasets/ds093.2/

CMIP5-AMIP, Historical, and RCP8.5 model ensembles
Centre for Environmental Data Analysis
https://archive.ceda.ac.uk/

References Cited

Adler, R. F., G. J. Huffman, A. Chang, R. Ferraro, P. Xie, and co-authors, 2003: The Version-2 Global Precipitation Climatology Project (GPCP) Monthly Precipitation Analysis (1979–Present). *J. Hydrometeor., 4*, 1147–1167, https://doi.org/10.1175/15257541(2003)004<1147:TVGPCP>2.0.CO;2.

Capotondi, A., A. T. Wittenberg, M. Newman, E. Di Lorenzo, J.-Y. Yu, and co-authors, 2015: Understanding ENSO Diversity. *Bull. Am. Meteor. Soc., 96*, 921–938, doi 10.1175/BAMS-D-13-00117.1.

Chiang, J. C. and A. H. Sobel, 2002: Tropical Tropospheric Temperature Variations Caused by ENSO and Their Influence on the Remote Tropical Climate. *J. Clim., 15*, 2616–2631, https://doi.org/10.1175/1520-0442(2002)015<2616:TTTVCB>2.0.CO;2.

Chung, E.-S., B. Soden, B. J. Sohn, and L. Shi, 2014: Upper-tropospheric moistening in response to anthropogenic warming. *Proc. Natl. Acad. Sci., 111*, 11,636–11,641, doi:10.1073/pnas.1409659111.

Coelho, C. A. and L. Goddard, 2009: El Niño–Induced Tropical Droughts in Climate Change Projections. *J. Clim., 22,* 10.1175/2009JCLI3185.1.

Dai A., K. E. Trenberth, & T. R. Karl, 1998: Global variations in droughts and wet spells: 1900–1995. *Geophys. Res. Lett., 25*, 3367–3370.

Dee, D. P., S. M. Uppala, A. J. Simmons, P. Berrisford, P. Poli, and co-authors, 2011: The ERA-Interim reanalysis: configuration and performance of the data assimilation system. *Q.J.R. Meteorol. Soc., 137*, 553–597. doi:10.1002/qj.828.

Guilyardi, E., A. Wittenberg, A. Fedorov, M. Collins, C. Wang, A. Capotondi, G. J. van Oldenborgh, and T. Stockdale, 2009: Understanding El Niño in ocean atmosphere general circulation models: Progress and challenges. *Bull. Am. Meteor. Soc., 90*, 325–340. https://doi.org/10.1175/2008BAMS2387.1

Hubert, L. J., P. Arabie, and J. J. Meulman, 2002: Linear unidimensional scaling in the L2-norm: Basic optimization methods using MATLAB. *J. Classif., 19*, 303–328, https://doi.org/10.1007/s00357-001-0047-5.

Huffman, G., D. Bolvin, D. Braithwaite, K. Hsu, R. Joyce, and P. Xie, 2014: Integrated Multi-Satellite Retrievals for GPM (IMERG), version 4.4. NASA's Precipitation Processing Center, accessed 1 March, 2015, ftp://arthurhou.pps.eosdis.nasa.gov/gpmdata/.

Hulme, M. A., 1992: A 1951–80 global land precipitation climatology for the evaluation of general circulation models. *Clim. Dyn., 7*, 57—72, https://doi.org/10.1007/BF00209609.

Hulme M., T.J. Osborn, and T.C. Johns, 1998: Precipitation sensitivity to global warming: comparison of observations with HadCM2 simulations. *Geophys. Res. Lett., 25*, 3379-3382.

Kumar, S., P. A. Dirmeyer, V. Merwade, T. DelSole, J. M. Adams, and D. Niyogi, 2013: Land use/cover change impacts in CMIP5 climate simulations: A new methodology and 21st century challenges. *J. Geophys. Res. Atmos., 118*, 6337– 6353, doi:10.1002/jgrd.50463.

Langenbrunner, B. and J. D. Neelin, 2013: Analyzing ENSO teleconnections in CMIP models as a measure of model fidelity in simulating precipitation, *J. Clim., 26*, 4431–4446, doi:10.1175/JCLI-D-12-00542.1.

Lintner, B. R., and J. C. H. Chiang, 2007: Adjustment of the remote tropical climate to El Niño conditions. *J. Clim., 20*, 2544—2557, doi:10.1175/JCLI4138.1.

Lintner, B. R., M. Biasutti, N. S. Diffenbaugh, J.-E. Lee, M. J. Niznik, and K. L. Findell, 2012: Amplification of wet and dry month occurrence over tropical land regions in response to global warming. *J. Geophys. Res.-Atmos., 117*, D11106, doi:10.1029/2012JD017499.

Liu, C., and R. P. Allan, 2013: Observed and simulated precipitation responses in wet and dry regions 1850–2100. *Environ. Res. Lett.* 8, 034002.

Lyon, B., 2004: The strength of El Niño and the spatial extent of tropical drought, *Geophys. Res. Lett., 31*, L21204, doi:10.1029/2004GL020901.

Lyon, B., and A. G. Barnston, 2005: ENSO and the Spatial Extent of Interannual Precipitation Extremes in Tropical Land Areas. *J. Clim., 18*, 5095–5109,https://doi.org/10.1175/JCLI3598.1

Nasrollahi, N., A. AghaKouchak, L. Cheng, L. Damberg, T. J. Phillips, C. Miao, K. Hsu, and S. Sorooshian, 2015: How well do CMIP5 climate simulations replicate historical trends and patterns of meteorological droughts? *Water Resour. Res., 51*, 2847–2864, doi:10.1002/2014WR016318.

Saha, S., S. Moorthi, H. Pan, X. Wu, J. Wang, and co-authors, 2010: The NCEP Climate Forecast System Reanalysis. *Bull. Amer. Meteor. Soc., 91*, 1015–1058, https://doi.org/10.1175/2010BAMS3001.1.

Saha, S., S. Moorthi, H. Pan, X. Wu, J. Wang and co-authors, 2012: NCEP Climate Forecast System Version 2 (CFSv2) Monthly Products, https://doi.org/10.5065/D69021ZF, Research Data Archive at the National Center for Atmospheric Research, Computational and Information Systems Laboratory, Boulder, Colo.

Schneider, U., A. Becker, P. Finger, A. Meyer-Christoffer, B. Rudolf, and M. Ziese, 2011: GPCC Full Data Reanalysis Version 6.0 at 2.5°: Monthly Land-Surface Precipitation from Rain-Gauges built on GTS-based and Historic Data. doi:10.5676/DWD_GPCC/FD_M_V7_250.

Taylor, K. E., 2001: Summarizing multiple aspects of model performance in a single diagram. *J. Geophys. Res., 106*, 7183–7192.

Taylor, K. E., R. J. Stouffer, and G. A. Meehl, 2012: An overview of CMIP5 and the experiment design. *Bull. Amer. Meteor. Soc., 93*, 485—498, doi: 10.1175/BAMS-D-11-00094.1.

Ukkola, A. M., A. J. Pitman, M. G. De Kauwe, G. Abramowitz, N. Herger, J. P. Evans, and M. Decker, 2018: Evaluating CMIP5 Model Agreement for Multiple Drought Metrics. *J. Hydrometeor., 19*, 969–988, https://doi.org/10.1175/JHM-D-17-0099.1.

Wilhite, D. A., and M. H. Glantz., 1985: Understanding the Drought Phenomenon: The Role of Definitions. *Drought Mitigation Center Faculty Publications. 20*, http://digitalcommons.unl.edu/droughtfacpub/20.

Willmott, C. J., and K. Matsuura, 2001: Terrestrial Air Temperature and Precipitation: Monthly and Annual Time Series (1950-1999) (Version 1.02). Center for Climatic Research, Department of Geography, University of Delaware.

Xie, P., and P. A. Arkin, 1997: Global Precipitation: A 17-Year Monthly Analysis Based on Gauge Observations, Satellite Estimates, and Numerical Model Outputs. *Bull. Amer. Meteor. Soc., 78*, 2539–2558, https://doi.org/10.1175/1520-0477(1997)078<2539:GPAYMA>2.0.CO;2.

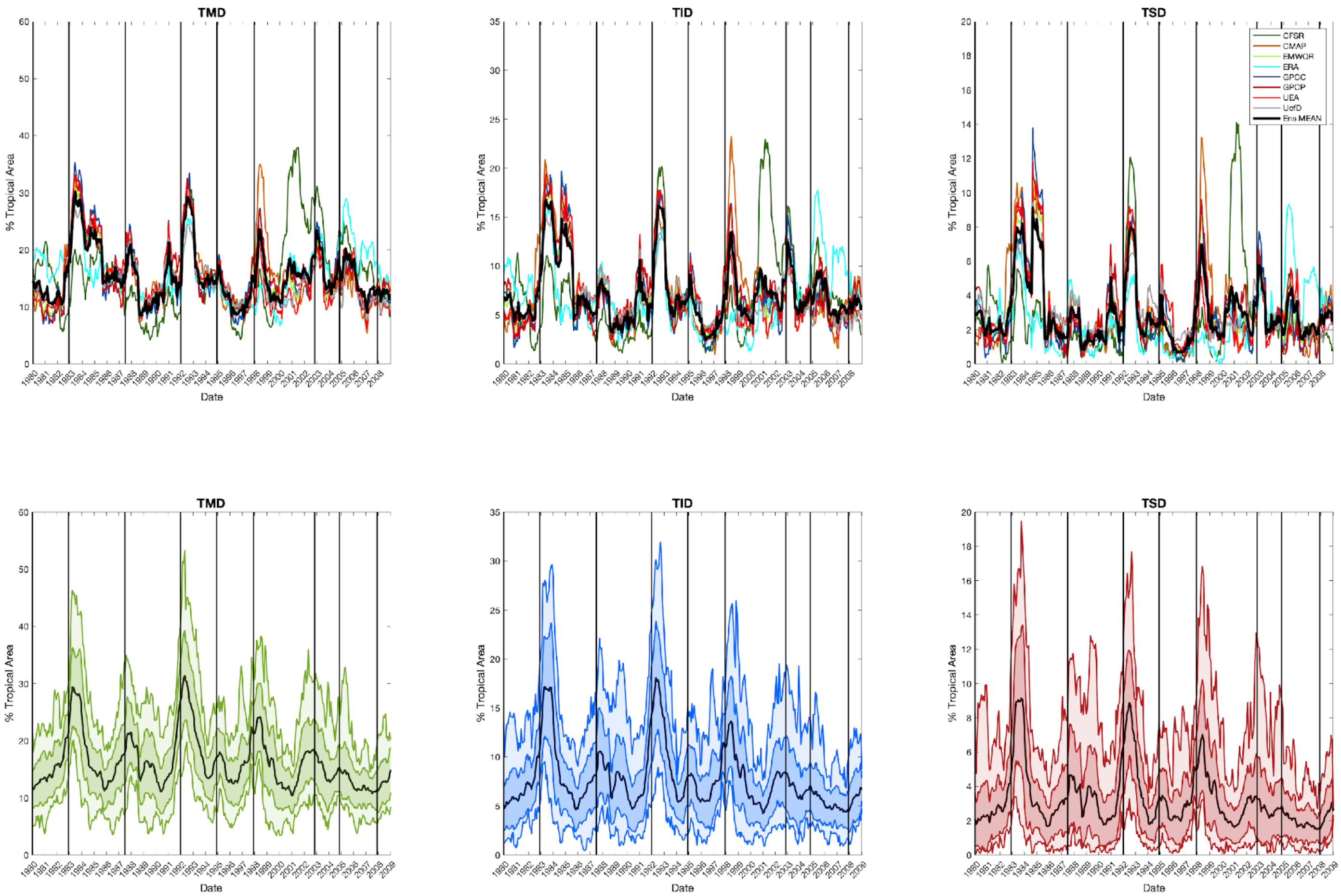

Figure 1: Timeseries of the fraction of tropical land region experiencing drought by category (moderate [TMD], left; intermediate [TID], middle; and severe [TSD], right; see text for definitions) from observations/reanalyses (top row) and prescribed SST (AMIP) simulations from CMIP5 (bottom row). For the observations/reanalyses, individual products are labeled with colored lines according to the legend, with the mean over the five observational products analyzed given by the thick black line. For the AMIP models, the model ensemble mean (MEM) corresponds to the thick black line, with the $\pm 1\sigma$ envelope of the MEM denoted by dark shading, and the maximum-minimum range of the models by light shading. Vertical lines in each plot correspond to the peaks of El Niño conditions.

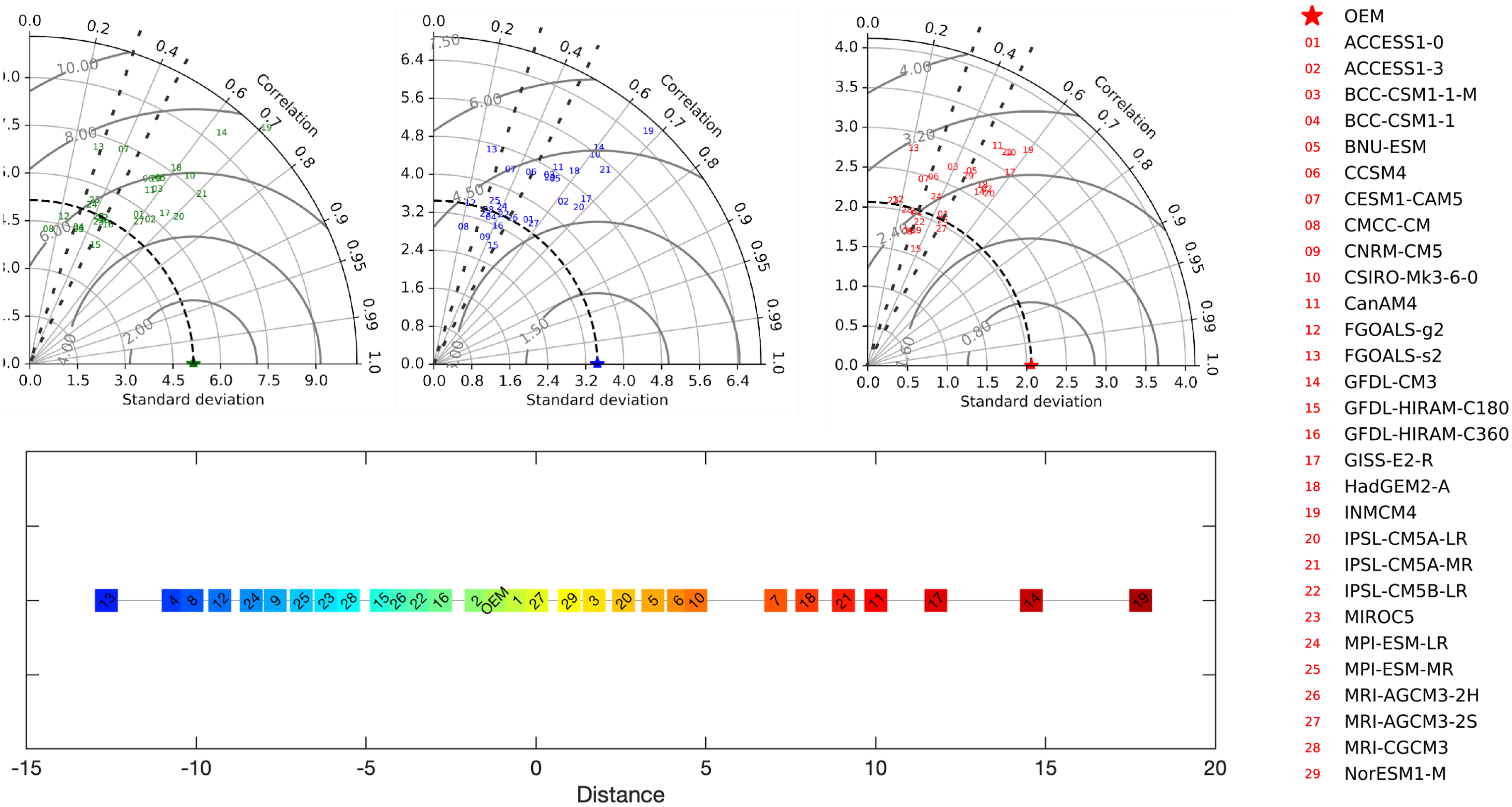

Figure 2. Quantitative comparison of the observational mean and AMIP models. The top row depicts Taylor plots for the categorical drought fraction timeseries of the AMIP models relative to mean of the observations shown in Figure 1 for the TMD (left), TID (middle), and TSD (right) categories. For each category, the observational mean (OEM) is shown by the star along the x-axis, while each model is labeled by its numerical value indicated in the legend. The bottom row depicts the LUS ordering of the models and the observed mean for the TMD category. The models are again labeled by numerical values according to the legend.

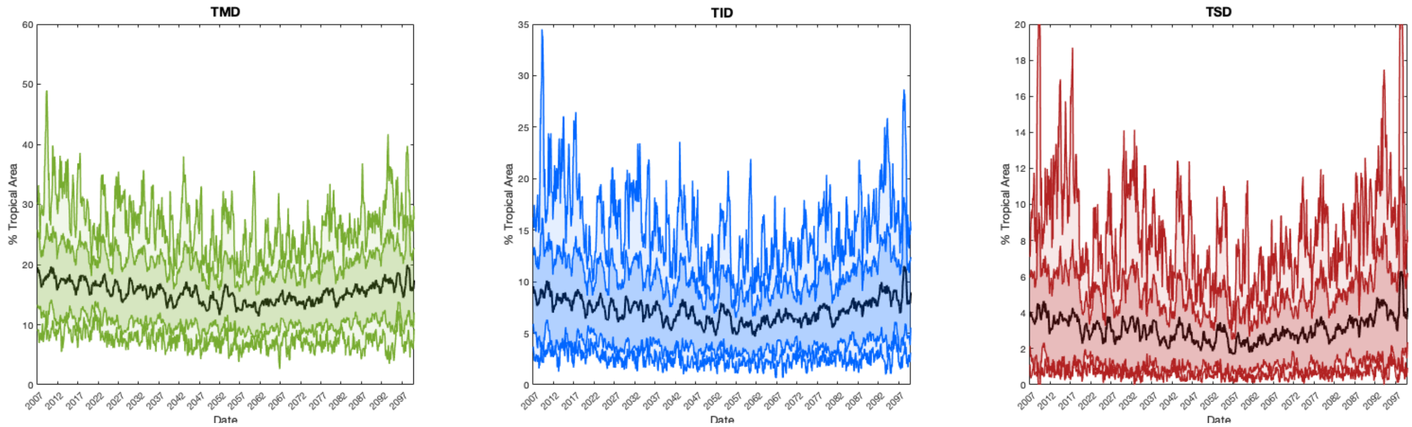

Figure 3. Categorical drought fraction timeseries (TMD, left; TID, middle; and TSD, right) for RCP8.5 projections. The model ensemble mean (MEM) corresponds to the thick black line, with the ±1σ envelope of the MEM denoted by dark shading, and the maximum-minimum range of the models by light shading.

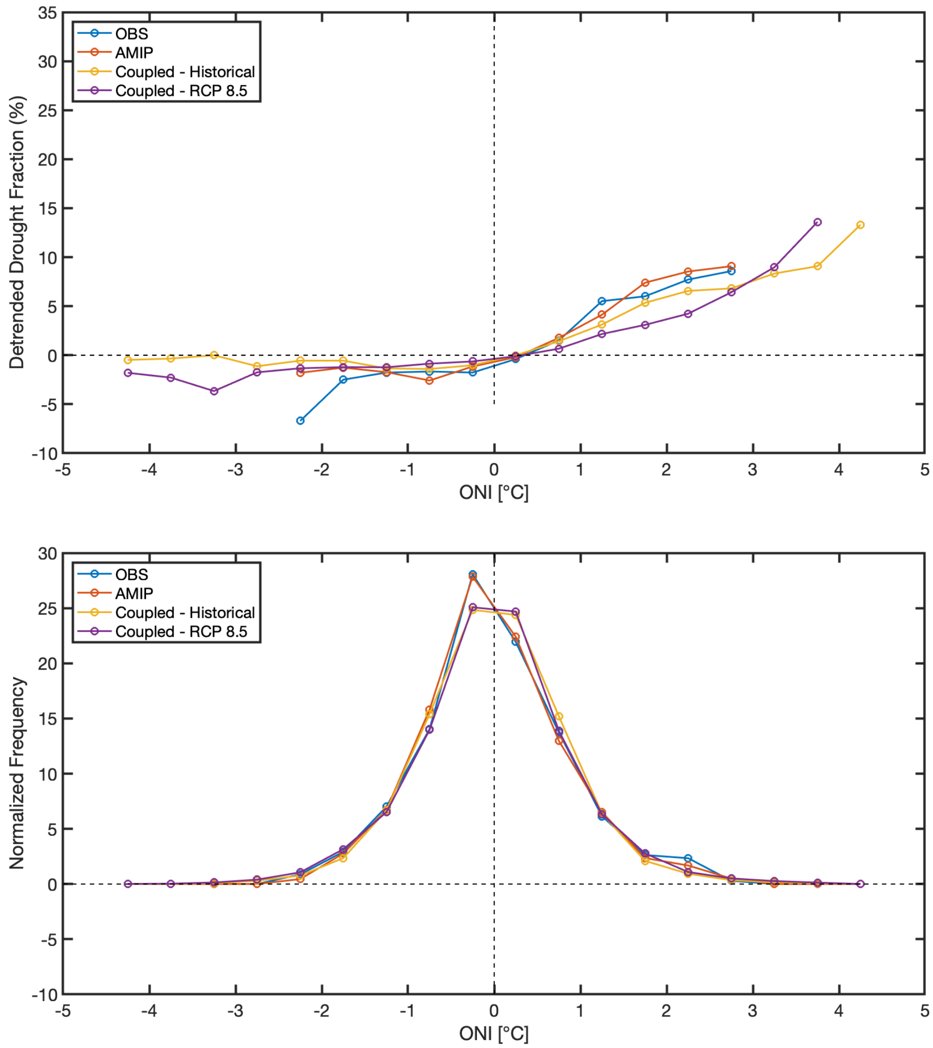

Figure 4. Histograms of detrended TMD fraction for observations and models vs. detrended ONI (top) and counts of detrended ONI values (bottom) in observations (and reanalyses; blue) and the AMIP (orange), coupled historic (orange), and RCP8.5 (purple) model ensembles. Prior to construction of these histograms, a moving 10-year (120-month) running mean is removed.